Droplet Impact Dynamics on Lubricant-Infused Superhydrophobic Surfaces: The Role of Viscosity Ratio

Jeong-Hyun Kim and Jonathan P. Rothstein*

Department of Mechanical and Industrial Engineering, University of Massachusetts Amherst, 160 Governors Drive, Amherst, Massachusetts 01003-2210, United States

ABSTRACT: In this study, the spreading and retraction dynamics of impacting droplets on lubricant-infused PTFE surfaces were investigated through high-speed imagery. Superhydrophobic Polytetrafluoroethylene (PTFE) surfaces with randomly rough microstructures were prepared by sanding PTFE. Several silicone oils with different viscosities were infused into the structures of superhydrophobic PTFE surfaces. A glycerin and water solution was used for the impacting droplets. The viscosity ratio between the impinging droplet and infused oil layer was varied from 0.06 to 1.2. The droplet impact dynamics on lubricant-infused surfaces were found to change as the viscosity of the infused silicone oil layer was decreased. These changes included an increase in the spreading rate of the droplet following impact, an increase to the maximum spreading diameter, and an increase to the retraction velocity after the droplet reached its maximum diameter. These variations in the impact dynamics were most significant as the viscosity ratio became larger than one and are likely due to the reduction of viscous losses between the oil and water phases during the spreading and retraction of the impacting droplet. Using a scaling analysis which takes into account the role of energy dissipation in the impact dynamics, all the data for the maximum diameter of the droplet on lubricant-infused PTFE surfaces were found to collapse onto a single master curve. Finally, measurements of the dynamic advancing and receding contact angle were made during spreading and retraction of the droplet. These measurements showed the expected Cox–Voinov–Tanner scaling of contact angle for the high oil viscosity, low viscosity ratio lubricant infused surfaces. However, like the superhydrophobic surface, little changes in either the dynamic advancing or receding contact angle were observed for droplets spreading on the surface infused with the lowest viscosity oil.
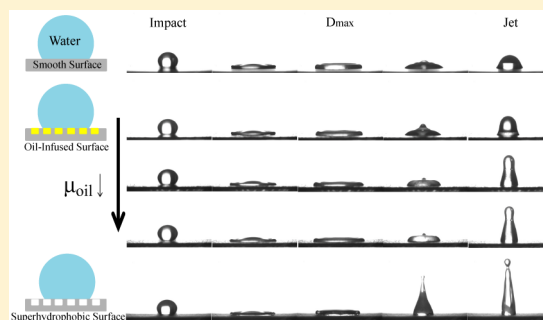
INTRODUCTION

The development of superhydrophobic surfaces was inspired by the extreme water repellency observed in plants[1] and insects[2,3] around the world. These superhydrophobic surfaces are composed of hydrophobic surfaces containing micrometer- and/or nanometer-sized surface structures. Because of surface tension, air can be trapped between peaks of surface roughness, thus preventing water from penetrating into the gaps or valleys between surface protrusions. The presence of the resulting air–water interface can increase the advancing contact angle with water toward 180° while eliminating contact angle hysteresis.[4–7] The air–water interface is nearly shear-free. As a result, superhydrophobic surfaces are useful in a number of promising applications such as laminar and turbulent drag reduction,[8–14] anti-icing,[15,16] and antifouling.[17,18] Unfortunately, there are a number of situations in which the great potential cannot be fully realized. For example, the air–liquid interface can collapse under large static and/or dynamic pressure[10,19] as well as the presence of any mechanical defects on the surface.[19,20] Furthermore, the air–water interface does not repel low surface tension liquids even under low static and/or dynamic pressure without the inclusion of special surface features like a re-entrant structure.[21]

Recent developments in lubricant-infused surfaces (LIS) have begun to address many of the implementation issues associated with superhydrophobic surfaces.[22,23] In LIS, an immiscible, incompressible, and low-viscosity lubricant is coated onto a superhydrophobic surface where it is deposited into the surface structure. Smith et al.[24] showed that depending on the interfacial tension among the oil, water, and surface, the lubricating oil will either become impregnated within the surface roughness leaving the tops of the roughness exposed to the water or the lubricating oil will fully encapsulate the surface features. The latter is beneficial for enhancing droplet mobility but is prone to faster lubricant depletion rates.[24] The incompressible lubricant layer resists large static pressure and repels various kinds of liquid including those with low surface tensions.[22] Furthermore, the lubricant layer was found to restore a liquid-repellent property after abrasion and impact of liquids unlike the air-infused superhydrophobic surfaces. A number of research groups have begun to investigate other potential uses of lubricant-infused superhydrophobic surfaces including for drag reduction, anti-icing, and antibacterial applications.[24–32]

For lubricant-infused surfaces, the effect of ratio between viscosity of the water, μ_w, and the oil phases, μ_o, is always an

Table 1. Wetting Parameters for PTFE Surfaces Tested

	SM	LIS 100	LIS 14	LIS 5	SHS
advancing contact angle, θ_A (deg)	111.5 ± 0.3	102.4 ± 1.1	101.8 ± 0.9	100.5 ± 0.7	155.5 ± 0.5
contact angle hysteresis, θ_H (deg)	34.4 ± 0.7	2.3 ± 1.3	4.1 ± 1.0	2.4 ± 1.1	4.4 ± 1.2
lubricant viscosity, μ_o (cP)		100	14	5	0.02
viscosity ratio, μ_w/μ_o		0.06	0.43	1.2	300

important factor to understand. On superhydrophobic surfaces filled with air, the viscosity ratio between water and air is approximately μ_w/μ_{air} = 55 at room temperature. This large viscosity ratio justifies the frequent assumption that the air–water interface is shear-free. Solomon et al.[29] showed that the frictional stress along a lubricant-infused surface can be reduced by increasing the viscosity ratio between the water and oil phases, μ_w/μ_0. Their measurement of LIS using a cone-and-plate rheometer showed a maximum drag reduction and a maximum slip length of 16% and 18 μm, respectively, at a viscosity ratio of μ_w/μ_o = 260.[29] Rosenberg et al.[30] recently showed drag reduction measurements on the lubricant-infused surface in the Taylor–Couette flow. They demonstrated that no drag reduction was attained at a viscosity ratio of μ_w/μ_o = 0.03. However, the drag reduction was found to increase from 5% to 14% as a viscosity ratio was increased from μ_w/μ_o = 0.67 to μ_w/μ_o = 2.7.[30] Viscosity ratio has also been shown to affect droplet impact dynamics on lubricant-infused surfaces. Recent studies by Lee et al.[33] and Hao et al.[34] demonstrated that the retraction of a droplet from a lubricant-infused surface after impact was delayed significantly by increasing the viscosity of the infused oil or, equivalently, by reducing the viscosity ratio between the impinging water droplet and the infused oil layer. No differences in spreading dynamics were observed. This could be because all of the viscosity ratios tested were quite small, $\mu_w/\mu_o \ll 1$. As a result, many of the possible differences in droplet spreading dynamics, especially for lubricant-infused surfaces where the viscosity ratio was well above $\mu_w/\mu_o > 1$, could not be observed.

In this paper, the spreading and retraction dynamics of droplet impacting on a series of lubricant-infused surfaces will be presenting. However, unlike previous studies, we will increase the viscosity ratio to values larger than one to more fully investigate the effect of the viscosity ratio on the spreading and retraction dynamics of impacting droplets on LIS. Our experimental results will be compared against a theoretical model which predicts the increase in the maximum diameter of droplet after impacting on lubricant-infused surfaces with increasing viscosity ratio and reduced oil viscosity.

■ EXPERIMENT

A standard experimental setup for the droplet impact studies was used. For the impinging droplets, a 55 wt % glycerin/water solution was used to increase the viscosity ratio. The aqueous glycerin droplets have an initial diameter of D_0 = 3.3 mm, a surface tension of σ_w = 67 mN/m, and a viscosity of μ_w = 6 mPa·s and were generated using a syringe pump (KD Scientific Model 100) from a syringe tip attached to plastic tubing and suspended a distance between 0 and 2 m above a leveled glass table. The droplets were accelerated by gravity, and their velocity at impact and exact diameter were measured through analysis of high-speed video camera (Phantom 4.2) images.

A series of test surfaces were placed at the impact location. These surfaces include a smooth polytetrafluoroethylene (PTFE) sheet purchased from McMaster-Carr which was used as a baseline along with a series of superhydrophobic and lubricant-infused surfaces. To produce the superhydrophobic surfaces, the smooth PTFE surface was roughened by sanding it with a 240-grit sandpaper to introduce

randomly rough microscale structures using the sanding technique described in Nilsson et al.[35] This grit size is known to produce a superhydrophobic surface with a high advancing contact angle, θ_A = 150°, and an extremely low contact angle hysteresis, $\theta_H = \theta_A - \theta_R$ = 4°.[35] In addition, these sanded PTFE surfaces have been shown to produce significant laminar drag reduction where tested in microfluidic channel experiments.[12] The superhydrophobic 240-grit sanded PTFE surface used here has been shown to result in a slip length of b = 20 μm. Note that the RMS surface roughness was estimated as 5.6 and 13.7 μm for the smooth PTFE surface and the sanded PTFE surfaces, respectively, based on the literature.[35]

Several silicone oils (Cannon Instrument Company) with the viscosity of μ_o = 5, 14, and 100 mPa·s and a surface tension of σ_o = 20 mN/m were infused into superhydrophobic PTFE surfaces by allowing the oil to wick into the surface topography. Excess silicone oil was removed by a doctor blade to produce uniform and thin oil layer. The resulting viscosity ratio between impacting droplets and the infused oil film, $\mu_{ratio} = \mu_w/\mu_o$, was varied between $0.06 < \mu_{ratio} < 1.2$. In microfluidic channel experiments,[32] the lubricant-infused surfaces have shown to produce increase in pressure drop reduction and slip length with increasing the viscosity ratio from μ_{ratio} = 0.2 to μ_{ratio} = 9.2. The pressure drop reduction was found to increase from 10% to 13% while the slip length was found to increase from 6 to 8 μm.[32] The advancing and receding contact angles of water on all three lubricant-infused PTFE surfaces were measured, and their properties are provided in Table 1. As shown in Table 1, advancing contact angles on the lubricant-infused surfaces were much smaller than the superhydrophobic surface although in both cases the contact angle hysteresis was quite small, $\theta_H < 4.5°$. The difference in advancing contact angle is due to the reduction in the interfacial tension as one replaces the air trapped within the superhydrophobic surface with silicone oil. For a superhydrophobic surface in the Cassie state, $\theta_{Cassie} = \cos^{-1}(-1 + \phi_S(1 + \cos\theta))$.[36] Here, ϕ_S is the fraction of the surface contact with the drop that is solid and θ is the contact angle made between the water and a smooth surface. For ϕ_S = 0, the superhydrophobic contact angle goes to 180°. For an impregnated lubricant-infused surface, $\theta_{LIS,i} = \cos^{-1}[(\gamma_{OA} - \gamma_{WO})/(\gamma_{OA} + \gamma_{WO}) + \phi_S(1 + \cos\theta)]$, where γ_{OA} is the interfacial tension between the oil and air, γ_{WO} is the interfacial tension between water and oil, and γ_{WA} is the interfacial tension between water and air. For a fully encapsulated lubricant-infused surface, the equilibrium contact angle of water is given by $\theta_{LIS,e} = \cos^{-1}[(\gamma_{OA} - \gamma_{WO})/(\gamma_{WO} + \gamma_{OA})]$.[33] As we will show in the Results and Discussion section, the difference in advancing and receding contact angle between the air-infused surface and lubricant-infused surfaces has a significant effect on the droplet impact dynamics.

The droplet impact velocity, U_0, was varied from 0.7 to 1.9 m/s by changing the height from which the droplet was released. The resulting Weber number at impact, $We = \rho_w U_0^2 D_0/\sigma_w$, thus ranged from $25 < We < 172$. Here, ρ_w is the density of the droplet, U_0 is the drop impact velocity, D_0 is the initial diameter of the droplet before impact, and σ_w is the surface tension of the droplet. The spreading and retraction dynamics of the droplets on each surface were recorded by a high-speed camera (Phantom V4.2) with a frame rate of 2200 Hz. A series of images were imported into the program ImageJ, and the evolution of the droplet diameter, spreading and retraction velocities, and the dynamic contact angle were measured as a function of time after impact. The frame containing the first contact of the droplets on the surfaces ($t \cong 0$ ms) is shown in the first column of Figure 1. This time is only as precise as the time between frames (~0.46 ms), and as seen in Figure 1, the first observed instance of impact is different for each measurement. In order to more accurately quantify the exact impact
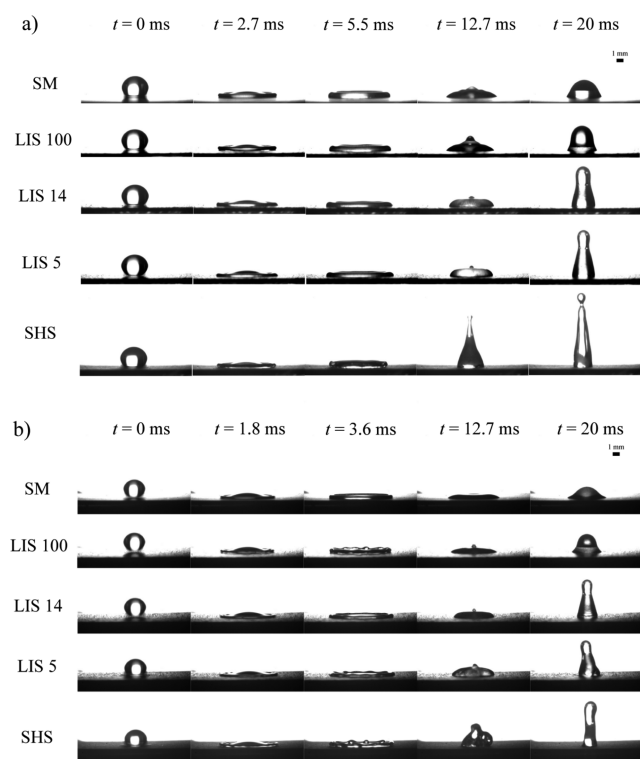
Figure 1. Time evolution of an aqueous glycerin drop (μ = 6 cP) impacting on a series of test surfaces at Weber numbers of (a) We = 52 and (b) We = 132. The surfaces include SM = smooth, SHS = superhydrophobic air-infused, and LIS = lubricant-infused. For the lubricant-infused surface, the viscosity of the silicone oil in cP is included following LIS.

time for later analysis, the distance between the center of the droplet and the testing surface was measured and, in combination with the impact velocity, used to calculate the exact time of impact for each experiment. In this way, the resolution of the impact time was reduced by a factor of nearly 10 to 0.06 ms for the We = 132 case and even better for lower Weber numbers. The droplet impact tests on each surface were conducted a minimum of three times at several different positions along the surface to improve the confidence in the repeatability of these experiments. From these measurements, a maximum uncertainty in the maximum droplet diameter, D_{max}, was calculated to be 0.15 mm, which is 4.6% of the initial droplet size (D_0 = 3.27 mm) while the maximum uncertainty of the droplet spreading and retraction velocities was calculated to be 0.022 m/s, which is 1.4% of the impact velocity (U_0 = 1.62 m/s) at We = 132.

■ RESULTS AND DISCUSSION

In Figure 1, a series of time-resolved images of spreading and retraction dynamics of droplets on the smooth, air-infused, and lubricant-infused PTFE surfaces are shown. Here, we provide two different Weber number cases, We = 52 and We = 132. The smooth PFTE surface (SM) can be considered a zero viscosity ratio experiment, $\mu_{rat} = \mu_w/\mu_o = 0$, while the air-infused superhydrophobic PTFE surface (SHS) represents the highest viscosity ratio case tested, $\mu_{rat} = \mu_w/\mu_o = 300$. Note that for the lubricant-infused PTFE surfaces (LIS) the number following "LIS" indicates the viscosity of the silicone oil used.

As can be seen in Figure 1, the droplet impact dynamics are qualitatively similar on all surfaces. Upon impact, the droplets deform to a pancake shape, reach a maximum diameter/deformation, and then retract to form a Worthington jet. The details of the dynamics of spreading and retraction of the

droplets were found to depend on the nature of the surface, rough or smooth, and the viscosity of the infused silicone oil. We will begin by discussing the dependence of the impact dynamics on the viscosity ratio of the three lubricant-infused surfaces before comparing the LIS results to the droplet impact on smooth and superhydrophobic PTFE surfaces. At all Weber numbers tested, including the two presented in Figure 1, the maximum spreading diameter of the droplet was found to increase with decreasing viscosity of the infused silicone oil layer. This can be observed directly from the third column of images in Figure 1, which was very close to the instant the droplet reached its maximum. This increase in maximum droplet diameter is a direct result of the reduced shear stress and large slip length that has been observed for the flow over lubricant-infused surfaces in the past.[29,30,32] As the viscosity of the silicone oil was decreased, the shear stress between the spreading droplet and the oil layer infused within the roughened PTFE surface was reduced. As a result, the reduction in energy dissipation during the droplet impact and subsequent spreading increased the maximum diameter of the droplet with decreasing oil viscosity. Note that the maximum spreading diameter observed for the highest viscosity silicone oil tested, LIS 100, was in fact very close to the measurement for droplet impacts on the smooth PTFE surface. This is likely because the viscosity ratio between the droplet and the lubricant infused in the LIS 100 surface was quite small and could be thought of as essentially zero, μ_{rat} = 0.06. As a result, little drag reduction is expected in this case during the spreading phase. Interestingly, the maximum diameter at the lowest viscosity lubricant-infused surface, LIS 5, did not consistently follow the trends of the superhydrophobic, air-infused case. We will discuss this observation in more detail later in the paper.

The differences in the droplet impact dynamics were examined more quantitatively by tracking the time evolution of the drop diameter as it spreads on each surface from the high-speed images. In order to remove the influence of a drop size variation, each measurement was nondimensionalized by the initial drop size. The results for low and high Weber number, We = 52 and We = 132, respectively, are presented in Figures 2a and 2b as a function of time. As seen in Figures 2a and 2b, the maximal deformation of the droplet was found to increase from D_{max}/D_0 = 2.29 to D_{max}/D_0 = 2.51 and from D_{max}/D_0 = 2.85 to D_{max}/D_0 = 3.02, respectively, as the viscosity of the silicone oil was decreased. As discussed previously, the reduction in shear stress at the oil−water interface with decreasing oil viscosity likely causes the increase in the diameter of the impacting droplets. The reduction in viscous dissipation during the spreading phase can also be observed in the spreading velocities. The spreading velocities were calculated from the droplet diameter data in Figure 2 and are presented in Figure 3. As seen in Figures 3a and 3b, the spreading velocities are initially close to the impact velocity (U_o = 1.0 m/s at We = 52 and U_o = 1.6 m/s at We = 132) during the first stage of the impact.[37] The spreading velocities then decrease over time as kinetic energy is converted to potential energy through interface deformation and is dissipated due to the shear at the oil−water interface. During the spreading phase, the droplet spreading velocity on the LIS 5 was consistently larger than the LIS 100. This was more obvious at We = 52 as shown in Figure 3a. No significant differences in spreading velocity were observed between the LIS 5 and LIS 14 cases. In order to make Figure 3 more readable, we have therefore chosen to

a)

b)
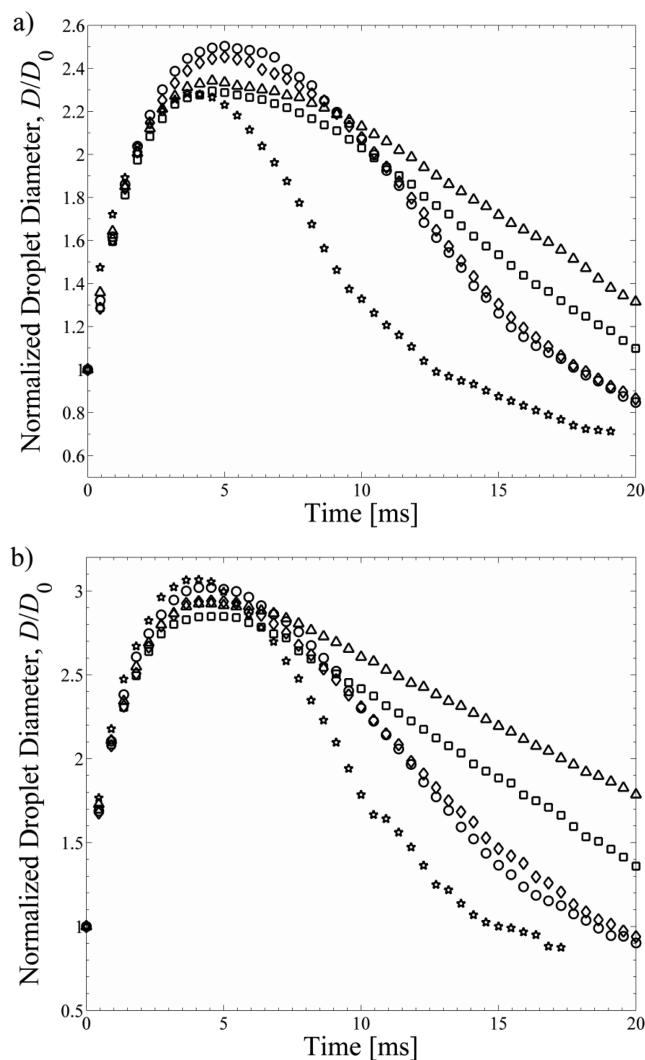
Figure 2. Time evolution of the diameter of the impacting aqueous glycerin drop normalized by the initial drop diameter at a Webber number of (a) $We = 52$ and (b) $We = 132$. The experimental data include lubricant-infused roughened PTFE surfaces with 5 cP silicone oil (●), 14 cP silicone oil (◆), and 100 cP silicone oil (■) as well as smooth PTFE surface (▲) and air-infused superhydrophobic PTFE surface (★).

a)

b)

Figure 3. Time evolution of the spreading (+ve) and retraction (−ve) velocities of droplet impacts on a number of different surfaces at a Weber number of (a) $We = 52$ and (b) $We = 132$. The experimental data include lubricant-infused roughened PTFE surfaces with 5 cP silicone oil (●) and 100 cP silicone oil (■) as well as smooth PTFE surface (▲) and air-infused superhydrophobic PTFE surface (★).

present the data for just LIS 5. Note that both the spreading diameter and velocity of the LIS 100 case approach the results from the smooth PTFE surface. This is a direct result of the large lubricant viscosity. It is also in agreement with the observation in the literature for $\mu_{ratio} \ll 1$.[33]

As was observed from the images in Figure 1a, at the lower Weber numbers tested, the droplets impacting on the LIS 5 surface were found to spread further than the air-infused superhydrophobic surface (SHS). This is surprising given that viscosity ratio between the droplet and the air is 250 times larger than for the LIS 5 surface. This clearly does not follow the trend observed for the three lubricant-infused surfaces which show a clear trend of the maximum diameter of the droplet and the spreading velocity which grows with increasing viscosity ratio or equivalently decreasing lubricant viscosity. In fact, at $We = 52$, the droplets impacting the LIS 5 surface spread nearly 10% further than the superhydrophobic surface. At the same Weber number, the peak spreading velocities are nearly 60% faster on the LIS 5 compared to the superhydrophobic

surface. Interestingly, both of those trends reverse at a Weber number of $We = 132$. These observations point to two important differences between superhydrophobic and liquid-infused surfaces. First, their advancing contact angles are very different, $\theta_A = 156°$ for SHS and $\theta_A = 101°$ for LIS 5. Because of its larger contact angle, we will show that deformation of the impacting droplet requires 54% more capillary energy for the same deformation. Second, even though the energy dissipation associated with droplet spreading is less for the superhydrophobic surfaces compared to the liquid-infused surfaces, there is additional energy dissipation for the superhydrophobic case associated with the dynamics of the Cassie to Wenzel transition beneath the impacting droplet. This dissipation mechanism does not exist for any of the LIS cases as the oil is incompressible and able to withstand the large pressures produced at impact. These differences appear to become less significant at larger impact velocities as the reduction in energy dissipation during droplet spreading on the superhydrophobic surfaces appears to dominate the spreading dynamics beyond impact Weber numbers of approximately $We > 100$.

In order to better understand the differences in the maximum spreading diameter between superhydrophobic and lubricant-infused surfaces, we considered the energy balance of an impacting droplet. In the calculations that follow, the shape of the droplet was assumed to be spherical before impact and was approximated as a flattened disk after impact. This second assumption is only truly valid for a highly deformed drop near the point of the maximum spreading as seen in Figure 1. The initial kinetic energy, KE_1, and surface energy, SE_1, of the spherical droplet are given by

$$KE_1 = \frac{1}{12}\pi\rho_w D_0{}^3 U_0{}^2 \tag{1}$$

$$SE_1 = \pi D_0{}^2 \sigma_w \tag{2}$$

The kinetic energy, KE_2, and surface energy, SE_2, of the disklike droplet after the impact are given by[37]

$$KE_2 = \frac{1}{24}\pi\rho_w D^3 U_S{}^2 \tag{3}$$

$$SE_2 = \frac{\pi}{4}D^2\sigma_w(1 - \cos\theta_A) \tag{4}$$

Here, D is instantaneous droplet diameter, U_S is the instantaneous droplet spreading velocity, and θ_A is static advancing contact angle. The kinetic energy of the spreading droplet after impact, KE_2, was calculated from a radial velocity profile calculated from a lubrication analysis. The droplet velocity was found to increase linearly with radial position from a value of zero at the center of the spreading drop, to a maximum of U_S at the spreading contact line. The kinetic energy in eq 3 was calculated by integrating $1/2\rho U^2(r)$ over the entire volume of the droplet. In the absence of any energy dissipation, we can set the sum of the kinetic plus interfacial energy before impact equal to its sum following impact, $(KE_1 + SE_1) = (KE_2 + SE_2)$. In this limit, the maximum spreading diameter can be calculated by setting the velocity of the spreading drop to zero, resulting in

$$\frac{D_{max}}{D_0} = \left(\frac{\rho_w D_0 U_0{}^2}{3\sigma(1 - \cos\theta_A)} + \frac{4}{1 - \cos\theta_A}\right)^{1/2}$$

$$= \left(\frac{We}{3(1 - \cos\theta_A)} + \frac{4}{1 - \cos\theta_A}\right)^{1/2} \tag{5}$$

Equation 5 demonstrates that for two drops impacting a surface at the same Weber number the maximum spreading diameter will be a function of the wettability of the surface and specifically the static advancing contact angle between the droplet and the interface. Thus, a nonwetting drop will not spread as far as a wetting drop because more energy is required to form the liquid solid interface beneath the spreading drop. The factor of $(1 - \cos\theta_A)$ in eq 5 partially explains why for the low Weber number experiments in Figure 2 droplets impacting the superhydrophobic surface did not spread as far as droplets impacting on the lubricant-infused surface or the smooth surface. However, to fully understand the difference between superhydrophobic and lubricant-infused surfaces, and to match the observed scaling of the maximum diameter with impact Weber number, we must also consider energy dissipation.[37,38] Equation 5 results in a scaling for the maximum droplet diameter that scales with Weber number to the one-half power, $D_{max}/D_0 \sim We^{1/2}$. However, Clanet et al.[38] demonstrated that

due to dissipation upon impact, a scaling of $D_{max}/D_0 \sim We^{1/4}$ is expected for low-viscosity liquids.[38] We will return to this scaling later in the text. Until then, we will measure the energy dissipation directly from the data in Figures 2 and 3.

Using energy conservation, the total accumulated energy dissipation at any time, DE, can be expressed as the difference between the instantaneous kinetic and interfacial energy and directly measured from the results of the drop impact experiments.

$$DE = (KE_1 - KE_2) + (SE_1 - SE_2) = \frac{\pi\rho_w D_0{}^3(2U_0{}^2 - U_S{}^2)}{24}$$
$$+ \frac{\pi\sigma_w[4D_0{}^2 - D^2(1 - \cos\theta_A)]}{4} \tag{6}$$

The energy dissipation in eq 6 includes both the energy losses accumulated during droplet spreading as well as the energy dissipated during droplet impact. The calculated dissipation energy on the LIS 5, SHS, and SM surfaces is shown in Figure 4 as a function of time and Weber number. The energy dissipated
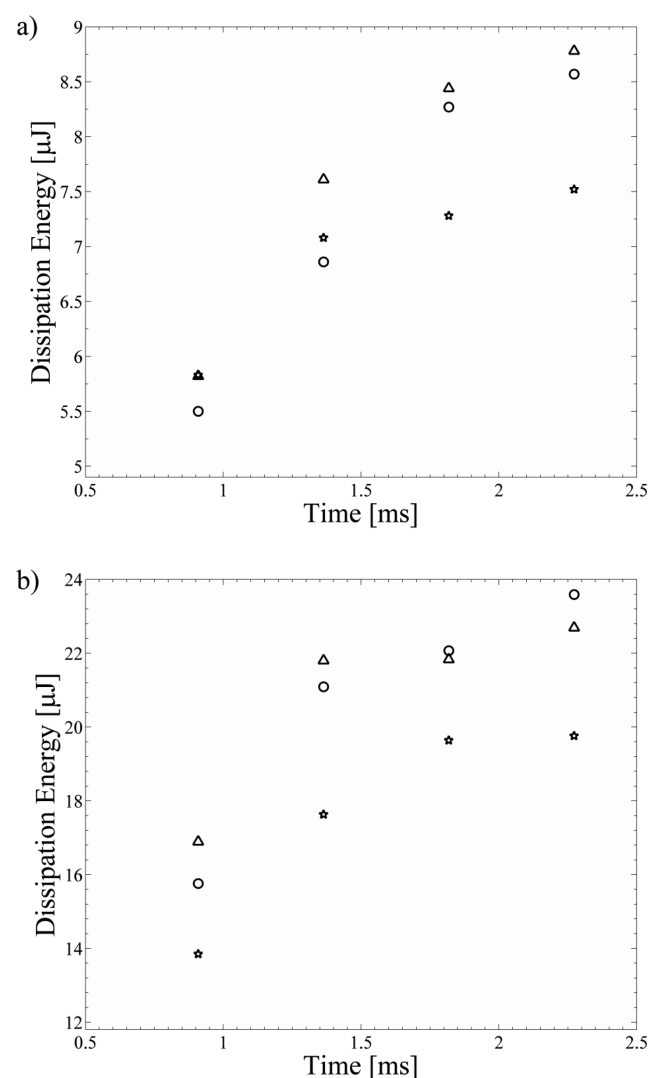
Figure 4. Energy dissipation as a function of time for droplet impacts at a Webber number of (a) $We = 52$ and (b) $We = 132$. The experimental data include impacts on lubricant-infused roughened PTFE surfaces with 5 cP silicone oil (●), smooth PTFE surfaces (▲), and air-infused superhydrophobic PTFE surfaces (★).

during the impact was determined by extrapolating the dissipation energy to the time of impact, $t = 0$, using a linear fit to the initial data in Figure 4. The energy dissipated during impact was calculated to be 2.2, 2.8, and 3.3 μJ for the SM, LIS 5, and SHS surfaces, respectively, at a Weber number of $We = 52$. At a Weber number of $We = 132$, the energy dissipated at impact was found to increase to 7.1, 5.1, and 6.3 μJ for the SM, LIS 5, and SHS surfaces, respectively. The energy dissipated at impact for the superhydrophobic surface was consistently about 20% larger than the LIS 5 over all Weber numbers tested. This suggests that the Cassie to Wenzel transition under the impacting droplet is a major source of additional energy dissipation during impact. However, it is interesting to note that even though the energy dissipation during impact was found to roughly double for the LIS and SHS surfaces as the Weber number was increased from $We = 52$ to $We = 132$, the total energy dissipated over the entire spreading time was found to increase by almost a factor of 3. Thus, with increasing Weber number, the dissipation upon impact appears to play a diminishing role in the overall spreading dynamics.

The dissipation rate on each surface can also be studied by either taking the derivative of the data in Figure 4 with time or simply visualizing the slope of the data. The dissipation rate directly related to the viscous losses associated with the droplet spreading on a solid, air-infused, or lubricant-infused surface. At lower Weber number, as seen in Figure 4a, the initial dissipation rate on the superhydrophobic surface was slightly smaller than the dissipation rate on LIS 5 and a full 40% smaller than the dissipation rate on the smooth surface. Similar observations were found for all Weber numbers tested. These observations are a direct result of the slip velocity and the associated reduction of viscous stress at the air−water and oil−water interface experienced during spreading.[12,32] The slip length is known to decrease with increasing viscosity of the lubricant.

Because of the energy dissipated at impact and the additional viscous losses during the spreading of the droplet, the initial droplet kinetic energy is not completely transformed to the surface energy.[38] During retraction of a nonwetting droplet, these losses can result in an incomplete or partial rebound of the droplet. The viscous losses reduce the kinetic energy available to drive droplet ejection. For the case of the superhydrophobic surface, the wetting transition from Cassie to Wenzel beneath the impacting drop can also greatly enhance adhesion during the final stages of Worthington jet formation making complete rebound less likely. By measuring the adhesion area on the test surfaces during Worthington jet formation, the amount of surface driven into the Wenzel state by the high pressures at impact can be estimated. For the Weber number of $We = 52$, the adhesion area was found to be $A_{C-W} = 3.3 \pm 0.1$ mm^2 or roughly one-third the projected area of the impacting drop, while for $We = 132$, $A_{C-W} = 3.3 \pm 0.2$ mm^2. Interestingly, no significant difference in the adhesion area was observed with increasing drop impact velocity, suggesting that the area under the drop that transitions from the Cassie to the Wenzel state during impact is not strongly dependent on impact speed.

An additional observation from Figure 2 is that the droplets appear to pause for a short time at their maximum diameter before retracting. Here, we define the time that the droplet pauses at its maximum diameter before retracting as its time delay. To quantify the time delay on each surface, the time difference between when the drop reaches 90% of its maximum

diameter during spreading and subsequently during retraction was measured and plotted in Figure 5. The first observation
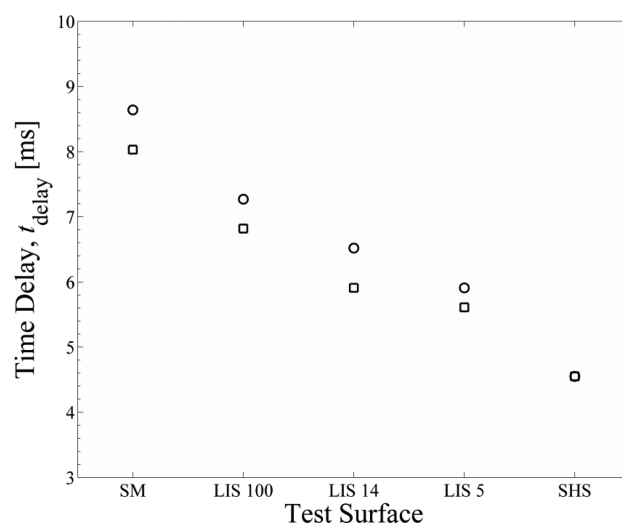
Figure 5. Time delay of impacting droplets at maximum spreading diameters. Data represent difference between the time to achieve 90% D_{max} during spreading and the time to reach 90% D_{max} during retraction of droplet from D_{max}. The data include impacts on different test surfaces at impact Weber numbers of $We = 52$ (●) and $We = 132$ (■).

from Figure 5 is that the superhydrophobic surface exhibits almost no pause at all with a delay time of only 4.5 ms that was found to be independent of impact Weber number. The second observation from Figure 5 is that the time delay is strongly dependent on the viscosity of the infused oil layer. The time delay decreases as the viscosity of the lubricants oil decreases, with the time delay doubling from 4.5 to 9 ms from the superhydrophobic to smooth case. The maximum uncertainty of the time delay was measured to be 0.5 ms on the SM and SHS surface while it was measured to be 0.4 ms on the LIS surfaces. As we will show, this pause at maximum deformation is directly related to the dynamic contact angle hysteresis between the glycerin and water solution and each of the surfaces tested. Both the advancing and receding dynamic contact angles of the impacting droplets on each of the five test surfaces were measured from the captured images using ImageJ. The results are plotted as a function of time in Figure 6a. The dynamic contact angle data were also replotted against the instantaneous spreading or retraction velocity of the droplet in Figure 6b. To eliminate the effect of changing surface tension or fluid viscosity, the data in Figure 6b are recast as the dimensionless capillary number, $Ca = \mu U/\sigma$, as is the norm in dynamic contact angle studies. Note that wherever possible, the dynamic contact angles measured at the same velocity were averaged in Figure 6b to improve the quality of the data and reduce the scatter. However, in some instances, especially for contact angles near 90°, due to the limited resolution of the images, the contact angles could not be measured with any great confidence. This is the case for the advancing contact angle on LIS 5, and as a result, only three data could be included in Figure 6. The maximum uncertainty of the dynamic contact angles for all other measurements was found to be ±3.7°.

As seen in Figures 6a and 6b, the advancing contact angles on the air-infused superhydrophobic surface remain constant at

a)

b)
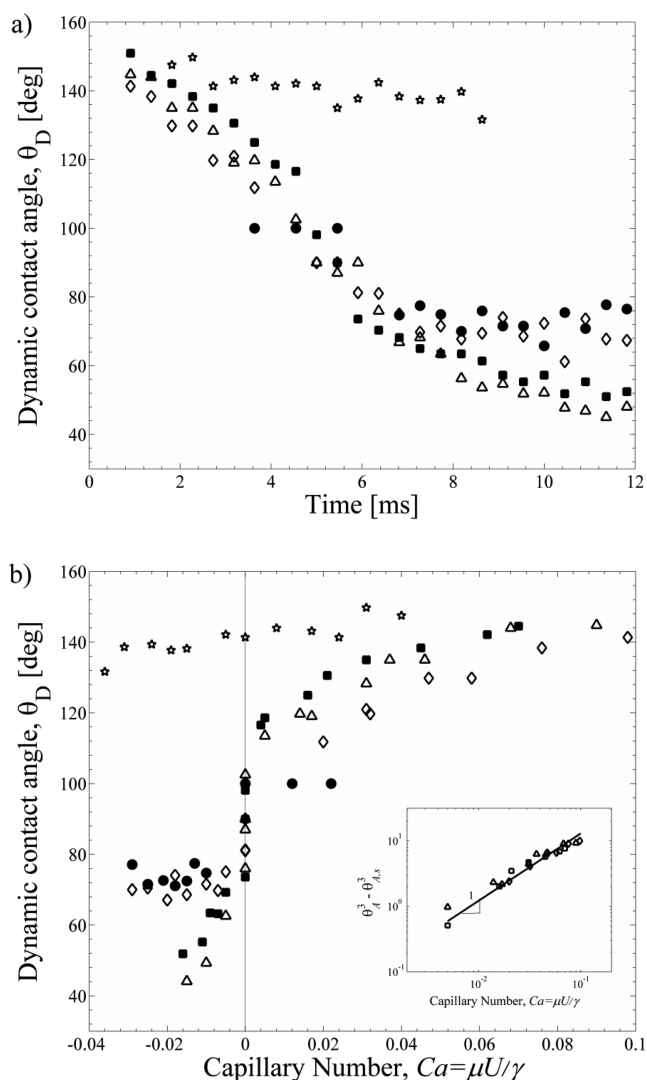
Figure 6. Dynamic contact angle measured during droplet impact on a number of different surfaces as a function of (a) time after impact and (b) the instantaneous capillary number during spreading (positive) and retraction (negative) at a Weber number of We = 52. The experimental data include lubricant-infused roughened PTFE surfaces with 5 cP silicone oil (●), 14 cP silicone oil (♦), and 100 cP silicone oil (■) as well as smooth PTFE surface (▲) and air-infused superhydrophobic PTFE surface (★).

θ_A = 145° independent of capillary number. This observation coincides with the result of dynamic contact angles measured by the drop impact test[39] and by a force wetting technique.[5] It also indicates that the kinetic energy of the impacting droplet on the air-infused surface is transformed into surface energy with no significant viscous dissipation from the surface.[38] Conversely, the advancing contact angles on smooth and lubricant-infused surfaces decreased over time or equivalently increased with increasing capillary number. This is the expected result for smooth surfaces where the advancing contact angle is known to increase with increasing velocity either due to hydrodynamic forces acting near the moving contact line[40,41] or due to molecular adsorption and desorption processes at the moving contact line.[40,42] In the case of the hydrodynamic Cox–Voinov–Tanner laws, $\theta_A{}^3 \propto Ca$.[43−45] The advancing contact angles on the SM, LIS 14, and LIS 100 surfaces were found to follow the Cox–Voinov–Tanner laws in our experiment as

shown in the inset of Figure 6b. Although it appears that the Cox–Voinov–Tanner law can predict the reaction in dynamic advancing contact angle for the low viscosity ratio lubricant-infused surfaces, the range of capillary numbers presented in Figure 6 is not sufficient as only 1 order of magnitude of capillary number data is spanned. As a result, the accuracy of the measurements is not sufficient for us to make a conclusive statement about the capillary number dependence of the data here. Unfortunately, this is especially true for the LIS 5 surface, which appears to behave more like the superhydrophobic surface with little to no dependence of contact angle on capillary number. Although these measurements represent the first dynamic wetting measurements on lubricant infused surfaces, forced wetting experiments, like those presented in Kim et al.,[5] are needed to fully understand the dynamic wetting process on lubricant-infused surfaces.

It is clear from Figure 1 that the type of surface, smooth or rough, and the viscosity of the air and silicone oil infused in the surface roughness not only affect the spreading dynamics but can also affect the retraction dynamics of the droplet. From the diameter evolution with time in Figure 2 and the velocities calculated in Figure 3, it can be observed that the retraction rate of the impacting droplets increases with decreasing viscosity of the infused silicone oil. The retraction rate of the highest viscosity silicone oil LIS 100 was found to approach the retraction rate of the droplet on the smooth PTFE surface. At these large lubricant viscosities, there is little difference between the shear stress generated between a drop spreading on a smooth surface and the lubricant-infused surface. In fact, the slip length is known to decrease linearly with increasing lubricant viscosity until it becomes too small to even measure.[29] As the viscosity of the oil is reduced to 5 mPa·s and the slip length increased, the retraction rate on the lubricant-infused surface was found to increase about by a factor of 2, approaching that of the superhydrophobic air-infused surface even though the viscosity ratios are still quite different, μ_{rat} = 1.2 compared to μ_{rat} = 300. However, even though the retraction rate of the least viscous silicone oil case, LIS 5, was similar to that of the superhydrophobic surface, as mentioned previously, the onset of retraction after reaching maximum spread diameter was delayed.

The delayed retraction dynamics on the LIS 5 can be best understood by inspecting the relationship between the droplet retraction velocity in Figure 3 and the dynamic receding contact angles in Figure 6. Here, we only focus on the lower Weber number case, We = 52. On the superhydrophobic air-infused surface, the dynamic receding contact angles maintained a constant value of θ_R = 140° even as the receding capillary number was increased by over an order of magnitude to Ca = 0.04. The resulting dynamic contact angle hysteresis is very small, θ_H = 5°. As a result, once the droplet had reached its maximum diameter, very little time and interfacial energy were needed to deform the contact line from its dynamic advancing contact angle to its dynamic receding contact angle. On the LIS 5, however, the dynamic receding contact angle was found to remain nearly constant at θ_R = 73° independent of capillary number for the velocities observed. This is significantly smaller than the static receding contact angle, $\theta_{R,S}$ = 98.1°. Thus, even though the lubricant-infused surfaces have little static contact angle hysteresis, the dynamic contact angle hysteresis for the LIS 5 is more than $\theta_H \geq 25°$. This observation reflects the viscous energy dissipation during flow which deforms the interface of the droplet during spreading. It is the need for the

droplet to transform from the dynamic advancing to receding contact angle after the maximal deformation of the droplet is reached that is responsible for the delay in the onset of droplet retraction. With increasing lubricant viscosity, an increasing in the dynamic advancing contact angle and a decrease in the dynamic receding contact angle was observed at a given capillary number. These dynamic contact angle measurements clearly show the effect that slip can have on the wetting dynamics in much the same way that has been observed for superhydrophobic surfaces.[5]

Finally, a common way in the literature to study the effects of different parameters on the droplet impact dynamics is to investigate changes to the maximum spreading diameter. In our previous discussion, we focused on just two Weber numbers, $We = 52$ and $We = 132$. In Figure 7, a comparison of the
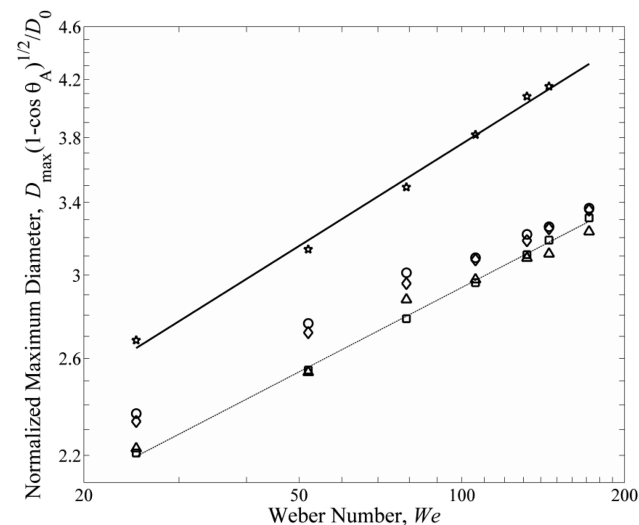
Figure 7. A log–log plot of maximum spreading diameter of the impacting aqueous glycerin drop normalized by the initial drop diameter as a function of Weber number. The experimental data include lubricant-infused roughened PTFE surfaces with 5 cP silicone oil (●), 14 cP silicone oil (◆), and 100 cP silicone oil (■) as well as smooth PTFE surface (▲) and air-infused superhydrophobic PTFE surface (★). The solid line of the air-infused case (★) indicates a scaling of $D_{max}/D_0 \sim We^{1/4}$ from theory,[38] while the dotted line of LIS 100 case (■) indicates a scaling of $D_{max}/D_0 \sim We^{1/5}$.

nondimensional maximum spreading diameter of the droplet after impact is shown for each surface tested for a wide range of Weber numbers between $20 < We < 200$. Note that in order to remove the effect of contact angle from maximum diameter comparison in Figure 7, eq 5 clearly indicates that the maximum spreading diameter should be multiplied by $(1 - \cos \theta_A)^{1/2}$. Normalized in this way, the droplet spreading on the superhydrophobic surfaces was found to far exceed the maximum droplet spreading diameter measured on either the smooth or the lubricant-infused surfaces for all the Weber numbers tested. This observation is consistent with the trends in the energy dissipation data in Figure 4. In all cases, the maximum spreading diameter was found to increase with increasing Weber number and, on the lubricant-infused surfaces, to increase with decreasing oil viscosity. As has been seen in the previous literature, the maximum spreading on the superhydrophobic surface was found to scale with $D_{max}/D_0 \sim We^{1/4}$.[38] To achieve the scaling, Clanet et al. hypothesized that the shape of the drop was a direct result of the enhanced gravity

the drop experienced as it impacted the substrate and decelerated. For low viscosity fluids, the shock of impact was found to result in a diameter growth that had a stronger dependence on impact velocity than high viscosity fluids $D_{max}/D_0 \sim U_0^{1/2}$ versus $D_{max}/D_0 \sim U_0^{1/5}$.[38] To arrive at the observed scaling, we start with the observation of Clanet et al. that a strong recirculation was observed in the spreading drop near the three-phase contact line.[38] Thus, rather than assuming all the volume of the drop is dissipating energy, including fluid at the center of the drop where the shear rate is minimal, we only consider the fluid within a torus of minor diameter $h/2$ and major diameter $D_{max}/2$ where the recirculation dominates and the shear rates are largest. The resulting energy dissipation scales like

$$\text{DE} \approx \Phi t_f V = \mu \left(\frac{2U_0}{h} \right)^2 \frac{D_{max}}{U_0} \frac{\pi^2}{4} h^2 D_{max} = \mu \pi^2 U_0 D_{max}^2 \tag{7}$$

Here Φ is the viscous dissipation function, t_f is the time of the experiment, V is the volume of the drop over which the viscous dissipation is occurring, and volume conservation is used to equate final to initial drop geometries, $h D_{max}^2 = 2/3 D_0^3$. Substituting into eq 6, we arrive at

$$\frac{D_{max}}{D_0} = \left(\frac{\frac{\rho_w D_0 U_0^2}{12} + \sigma_w}{\mu \pi U_0 + \frac{\sigma_w (1 - \cos \theta_A)}{4}} \right)^{1/2} = \left(\frac{Re + \frac{12}{Ca}}{12\pi + \frac{3(1 - \cos \theta_A)}{Ca}} \right)^{1/2} \tag{8}$$

which gives the observed scaling of $D_{max}/D_0 \sim U_0^{1/2}$ in the limit of moderate to large capillary numbers. Of course, this analysis does not take into account the slip at the air–water or oil–water interface, and although the scaling will remain the same, it must be extended to obtain the appropriate prefactors for each term within eq 8. In what follows, we will focus on lubricant-infused surfaces to simplify the notation and the discussion; however, it should be noted that the analysis is equally applicable to superhydrophobic surfaces.

For the liquid (or air) infused surfaces, the viscous energy dissipation to account for the oil (or air) layer on the surface can be estimated as $\text{DE} \approx \mu_w \pi^2 (U_0 - U_I) D_{max}^2$. Here, U_I is interfacial velocity at the oil–water (or air–water) interface. The interfacial velocity can be calculated to be $U_I = (t\mu_w/(h\mu_o + t\mu_w))U_0$ by matching the shear stress in the oil (or air) phase to the shear stress in the water phase at the interface. Here t is the oil (or air) film thickness. By equating the initial impact kinetic and surface energy to the final surface and dissipation energy, $KE_1 + SE_1 = SE_2 + DE$, it can be shown that the maximum spreading diameter depends on droplet geometry, viscosity ratio between the water and oil (or air) phase, Reynolds number, and capillary number:

$$\frac{D_{max}}{D_0} = \left(\frac{Re + \frac{12}{Ca}}{12\pi \left[1 + \left(\frac{t}{h} \right) \left(\frac{\mu_w}{\mu_o} \right) \right]^{-1} + \frac{3(1 - \cos \theta_A)}{Ca}} \right)^{1/2} \tag{9}$$

Equation 9 can be written in terms of the Weber number by replacing the Reynolds number with $Re = \sqrt{We}/Oh$, where $Oh = \mu/\sqrt{\rho \sigma D_0}$ is the Ohnesorge number. Note that we obtain the same scaling with velocity or Weber number found by Clanet et al.,[33,38] but with an expression that is modified by

the viscosity ratio. Although this does not exactly match the experimentally observed scaling of $We^{1/5}$ or $U^{2/5}$ observed for the lubricant infused surfaces, it does allow us to better understand the dependence of maximum spreading diameter on the infused oil viscosity. Unfortunately, at this moment, it is unclear what the physical reason is for the observed difference in the scaling of the maximum spreading diameter on the lubricant-infused surfaces and those observed for super-hydrophobic surfaces and predicted by theory. It should be noted that a recent paper by Lee et al.[46] addressed the question of whether there is a universal scaling for droplet impacts. By systematically studying the experimental literature, they proposed scaling that smoothly transitions from the low impact velocity regime where $D_{max}/D_0 \sim U^{1/5}$ to the high impact velocity regime where $D_{max}/D_0 \sim U^1$ with a single fitting parameter. This means that according to their model, any scaling between these two limits is feasible.[46]

In order to fit the scaling analysis in eq 9 to the data in Figure 7, the oil film thickness was assumed to be similar order of RMS surface roughness, $t = 14\ \mu m$,[35] and the thickness of the maximum spreading droplet, h, is calculated from the captured image. With this assumption, the prefactor becomes approximately $t/h \sim 0.12$. To test the scaling, the data in Figure 7 was replotted as $[D_{max}/D_0]/[1 + 0.12\mu_{ratio}]^{0.5}$ representing the limit when capillary number is large and presented in Figure 8. All
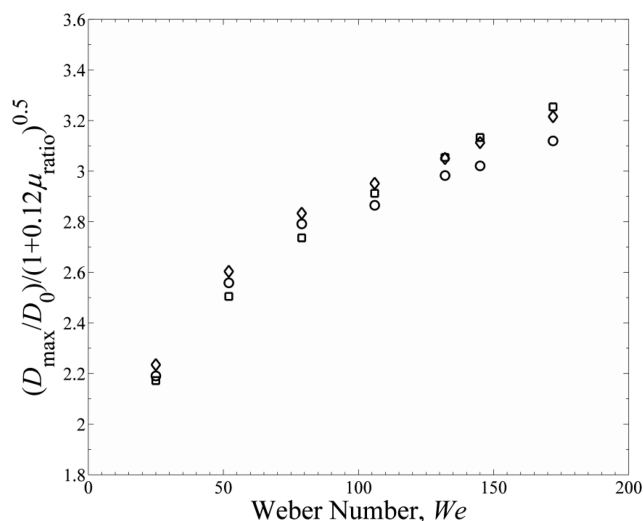
Figure 8. A scaling analysis for the maximum diameter of the aqueous glycerin drop normalized by the initial drop diameter as a function of Weber number. The experimental data include sanded lubricant-infused PTFE surfaces with 5 cP silicone oil (●), 14 cP silicone oil (◆), and 100 cP silicone oil (■). All the data collapse with the selection of $t/h = 0.12$.

the lubricant-infused surface data were found to collapse to within 5% onto a master curve. This scaling also explains why previous studies where the viscosity ratio was much less than one, $\mu_{ratio} \ll 1$, observed little to no change in the maximum spreading diameter of the impacting droplet.[33,34] For those experiments, $(t/h)(\mu_w/\mu_o) \ll 1$, and as a result, the effect of the infused oil layer can be ignored. For these cases of low viscosity ratio, eq 9 reverts to eq 8.

■ CONCLUSION

The spreading and retraction dynamics on lubricant-infused PTFE surfaces were investigated through high-speed imaging.

The lubricant-infused PTFE surfaces were prepared by sanding the smooth PTFE surface with 240-grit sandpapers and infusing the silicone oils into the microstructures of the surface. The viscosity of infused silicone oil was varied to investigate the effect of the viscosity ratio between the impinging droplet and the infused lubricant layer. The evolution of the droplet diameter, droplet spreading and retraction velocities, and the dynamic contact angles were measured as a function of time after impact.

The maximum spreading diameter of the droplet on lubricant-infused surfaces was found to increase with decreasing viscosity of the infused silicone oil. Furthermore, the droplet spreading velocities became larger as the oil viscosity was reduced. These increases in the maximum droplet diameter and the droplet spreading velocities resulted from the presence of a finite slip length and the reduction in shear stress at the oil–water interface on lubricant-infused surfaces. The results for the largest oil viscosity tested were indistinguishable from experiments performed on a smooth PTFE surface, showing the importance of increasing the viscosity ratio between the droplet and the infused oil phase to a value as large as possible. These differences with oil viscosity were not observed in previous studies because the oil viscosity was large and the resulting viscosity ratio was much less one, $\mu_w/\mu_o \ll 1$, in all cases.[33,34] This point is reinforced by a scaling analysis which was able to collapse the maximum diameter data onto a master curve when it was replotted as $D_{max}/D_0 = [1 + (t/h)(\mu_w/\mu_o)]^{1/2}We^{1/4}$.

Interestingly, significant and perhaps nonintuitive differences were observed in the maximum droplet diameter between the least viscous silicone oil case, LIS 5, and the air-infused superhydrophobic surface, SHS. At the lower Weber numbers tested, the maximum droplet diameter on the LIS 5 was found to be larger than that of the SHS even though the viscosity of the oil infused into the surface features of the LIS 5 was 250 times larger than the air infused into the surface features of the SHS case. This was shown to be due, in part, to the larger advancing contact angle on the superhydrophobic surface. However, it was also shown that a significant amount of energy was dissipated during the impact of a droplet on the SHS due to a wetting transition from the superhydrophobic Cassie state to the fully wetted Wenzel state induced by the large pressures produced beneath the drop. The presence of the incompressible oil in the lubricant-infused surface was found to mitigate these losses while still producing slip at the oil–water interface, thus resulting in a larger fraction of the initial kinetic energy available to deform the droplet to a greater maximum droplet diameter. As the Weber number was increased, the energy dissipation at impact was found to grow more slowly with Weber number than the energy dissipation during spreading. As a result, at $We = 100$, the maximum spreading droplet diameter on the superhydrophobic surface was found to surpass the lubricant-infused surfaces.

The retraction rate of the droplet on lubricant-infused surfaces was also found to increase with decreasing lubricant viscosity. The retraction rate on the LIS 5 approached that of the SHS; however, a significant difference in the time between reaching maximum diameter and beginning of the retraction was observed between the LIS 5 and the SHS. Once the droplet reached the maximum deformation, the motion of the droplet was observed to pause as the contact angles decreased from the dynamic advancing to the dynamic receding contact angle. Because the dynamic contact angle hysteresis on the SHS was extremely low, $\theta_H = 5°$, the observed delay time was quite

small, t_{delay} < 5 ms. However, even though the static contact angle hystereses on the lubricant-infused surfaces were all similar to the SHS and less than θ_H < 4°, the contact angle hystereses observed during spreading were all found to be much larger than the static case, θ_H > 25°. As a result, an increase in contact angle hysteresis and delay time was observed with increasing oil viscosity. Variation in contact angle with spreading velocity is known to occur due to viscous losses near the moving contact line.

Using the data from the droplet impact experiments, the first ever measurements of the dynamic advancing and dynamic receding contact angle were made for liquids spreading on lubricant-infused surfaces. The advancing contact angles on the smooth surface and both the LIS 14 and LIS 100 surfaces were found to increase with increasing capillary number. Furthermore, the advancing contact angles on the surfaces were all found to follow the expected Cox–Voinov–Tanner laws, $\theta_A{}^3 \propto Ca$. However, the onset of growth in the contact angle was delayed as the viscosity of the lubricant was decreased. The dynamic advancing contact angle on the LIS 5 surface did not follow the expected scaling laws but instead showed little to no growth in the contact angle with increasing capillary number. This behavior was similar to the observations for droplet spreading on superhydrophobic surfaces and is known to be a result of the large slip length and reduced shear stress near the moving contact line.[5] Similar observations were made for the dynamic receding contact angle which was found to decrease with an increasingly negative capillary number. Note, however, that the receding angle appeared to be more sensitive to lubricant viscosity than the advancing angle. These differences are the driving force behind the increase in observed dynamic contact angle hysteresis with increasing oil viscosity. Although these measurements are an important beginning, forced wetting experiments over a wider range of capillary numbers are needed to fully understand the dynamic wetting process on lubricant-infused surfaces.

■ AUTHOR INFORMATION

Corresponding Author
*E-mail: rothstein@ecs.umass.edu (J.P.R.).

Notes
The authors declare no competing financial interest.

■ REFERENCES

(1) Barthlott, W.; Neinhuis, C. Purity of the sacred lotus, or escape from contamination in biological surfaces. *Planta* **1997**, *202*, 1–8.
(2) Gao, X.; Jiang, L. Water-repellent legs of water striders. *Nature* **2004**, *432*, 36.
(3) Bush, J. W. M.; Hu, D. L.; Prakash, M. The Integument of Water-walking Arthropods: Form and Function. *Adv. Insect Physiol.* **2007**, *34*, 117–192.
(4) Gao, L.; McCarthy, T. J. A perfectly hydrophobic surface (theta(A)/theta(R) = 180°/180°). *J. Am. Chem. Soc.* **2006**, *128* (28), 9052–9053.
(5) Kim, J.-H.; Kavehpour, H. P.; Rothstein, J. P. Dynamic contact angle measurements on superhydrophobic surfaces. *Phys. Fluids* **2015**, *27*, 032107.
(6) Oner, D.; McCarthy, T. J. Ultrahydrophobic surfaces: Effects of topography length scales on wettability. *Langmuir* **2000**, *16*, 7777–7782.

(7) Quere, D. Non-sticking drops. *Rep. Prog. Phys.* **2005**, *68* (11), 2495–2532.
(8) Ou, J.; Perot, J. B.; Rothstein, J. P. Laminar drag reduction in microchannels using ultrahydrophobic surfaces. *Phys. Fluids* **2004**, *16*, 4635–4660.
(9) Ou, J.; Rothstein, J. P. Direct velocity measurements of the flow past drag-reducing ultrahydrophobic surfaces. *Phys. Fluids* **2005**, *17*, 103606.
(10) Rothstein, J. P. Slip on Superhydrophobic Surfaces. *Annu. Rev. Fluid Mech.* **2010**, *42*, 89–109.
(11) Srinivasan, S.; Choi, W.; Park, K.-C.; Chhatre, S. S.; Cohen, R. E.; McKinley, G. H. Drag reduction for viscous laminar flow on spray-coated non-wetting surfaces. *Soft Matter* **2013**, *9*, 5691–5702.
(12) Song, D.; Daniello, R.; Rothstein, J. P. Drag reduction using superhydrophobic sanded Teflon surfaces. *Exp. Fluids* **2014**, *55*, 1783.
(13) Truesdell, R.; Mammoli, A.; Vorobieff, P.; van Swol, P.; Brinker, C. J. Drag reduction on a patterned superhydrophobic surface. *Phys. Rev. Lett.* **2006**, *97*, 044504.
(14) McHale, G.; Shirtcliffe, N. J.; Evans, C. R.; Newton, M. I. Terminal velocity and drag reduction measurements on superhydrophobic spheres. *Appl. Phys. Lett.* **2009**, *94*, 064104.
(15) Farhadi, S.; Farzaneh, M.; Kulinich, S. A. Anti-icing performance of superhydrophobic surfaces. *Appl. Surf. Sci.* **2011**, *257*, 6264–6269.
(16) Cao, L.; Jones, A. K.; Sikka, V. K.; Wu, J.; Gao, D. Anti-Icing Superhydrophobic Coatings. *Langmuir* **2009**, *25* (21), 12444–12448.
(17) Zhang, H.; Lamb, R.; Lewis, J. Engineering nanoscale roughness on hydrophobic surface-preliminary assessment of fouling behavior. *Sci. Technol. Adv. Mater.* **2005**, *6*, 236–239.
(18) Genzer, J.; Efimenko, K. Recent developments in super-hydrophobic surfaces and their relevance to marine fouling: a review. *Biofouling* **2006**, *22*, 339.
(19) Bocquet, L.; Lauga, E. A smooth future? *Nat. Mater.* **2011**, *10*, 334–337.
(20) Quere, D. Wetting and roughness. *Annu. Rev. Mater. Res.* **2008**, *38*, 71–99.
(21) Liu, T. L.; Kim, C.-J. C. Turning a surface superrepellent even to completely wetting liquids. *Science* **2014**, *346*, 1096–1100.
(22) Wong, T.-S.; Kang, S. H.; Tang, S. K. Y.; Smythe, E. J.; Hatton, B. D.; Grinthal, A.; Aizenberg, J. Bioinspired Self-repairing slippery surfaces with pressure-stable omniphoicity. *Nature* **2011**, *477*, 443–447.
(23) Lafuma, A.; Quere, D. Slippery pre-suffused surfaces. *Europhys. Lett.* **2011**, *96*, 56001.
(24) Smith, J. D.; Dhiman, R.; Anand, S.; Reza-Garduno, E.; Cohen, R. E.; McKinley, G. H.; Varanasi, K. K. Droplet mobility on lubricant-impregnated surfaces. *Soft Matter* **2013**, *9*, 1772–1780.
(25) Wexler, J. S.; Jacobi, I.; Stone, H. A. Shear-Driven Failure of Liquid-Infused Surfaces. *Phys. Rev. Lett.* **2015**, *114*, 168301.
(26) Kim, P.; Wong, T.-S.; Alvarenga, J.; Kreder, M. J.; Adorno-Martinez, W. E.; Aizenberg, J. Liquid-Infused Nanostructured Surfaces with Extreme Anti-Ice and Anti-Frost Performance. *ACS Nano* **2012**, *6*, 6569–6577.
(27) Epstein, A. K.; Wong, T.-S.; Belisle, R. A.; Boggs, E. M.; Aizenberg, J. Liquid-infused structured surfaces with exceptional anti-biofouling performance. *Proc. Natl. Acad. Sci. U. S. A.* **2012**, *109*, 13182–13187.
(28) Subramanyam, S. B.; Rykaczewski, K.; Varanasi, K. K. Ice Adhesion on Lubricant-Impregnated Textured Surfaces. *Langmuir* **2013**, *29*, 13414–13418.
(29) Solomon, B. R.; Khalil, K. S.; Varanasi, K. K. Drag Reduction using Lubricant-Impregnated Surfaces in Viscous Laminar Flow. *Langmuir* **2014**, *30*, 10970–10976.
(30) Rosenberg, B. J.; Van Buren, T.; Fu, M. K.; Smits, A. J. Turbulent drag reduction over air- and liquid-impregnated surfaces. *Phys. Fluids* **2016**, *28*, 015103.
(31) Wexler, J. S.; Grosskopf, A.; Chow, M.; Fan, Y.; Jacobi, I.; Stone, H. A. Robust liquid-infused surfaces through patterned wettability. *Soft Matter* **2015**, *11*, 5023–5029.

(32) Kim, J.-H.; Rothstein, J. P. Delayed Lubricant Depletion on Liquid-Infused Randomly Rough Surfaces. *Exp. Fluids* **2016**, *57* (5), 81.

(33) Lee, C.; Kim, H.; Nam, Y. Drop Impact Dynamics on Oil-Infused Nanostructured Surfaces. *Langmuir* **2014**, *30* (28), 8400−8407.

(34) Hao, C.; Li, J.; Liu, Y.; Zhou, X.; Liu, Y.; Liu, R.; Che, L.; Zhou, W.; Sun, D.; Li, L.; Xu, L.; Wang, Z. Superhydrophobic-like tunable droplet bouncing on slippery liquid interfaces. *Nat. Commun.* **2015**, *6*, 7986.

(35) Nilsson, M.; Daniello, R.; Rothstein, J. P. A novel and inexpensive technique for creating superhydrophobic surfaces using Teflon and sandpaper. *J. Phys. D: Appl. Phys.* **2010**, *43*, 045301.

(36) Cassie, A. B. D.; Baxter, S. Wettability of porous surfaces. *Trans. Faraday Soc.* **1944**, *40*, 546−551.

(37) Pasandideh-Fard, M.; Qiao, Y. M.; Chandra, S.; Mostaghimi, J. Capillary effects during droplet impact on a solid surface. *Phys. Fluids* **1996**, *8* (3), 650−659.

(38) Clanet, C.; Beguin, C.; Richard, D.; Quere, D. Maximal deformation of an impacting drop. *J. Fluid Mech.* **2004**, *517*, 199−208.

(39) Bayer, I. S.; Megaridis, C. M. Contact angle dynamics in droplets impacting on flat surfaces with different wetting characteristics. *J. Fluid Mech.* **2006**, *558*, 415−449.

(40) Berg, J. C. *Wettability*; Marcel Dekker, Inc.: New York, 1993; p 531.

(41) Blake, T. D. The physics of moving wetting lines. *J. Colloid Interface Sci.* **2006**, *299*, 1−13.

(42) Blake, T. D.; Haynes, J. M. Kinetics of liquid/liquid displacement. *J. Colloid Interface Sci.* **1969**, *30* (3), 421−423.

(43) Tanner, L. H. The spreading of silicone oil drops on horizontal surfaces. *J. Phys. D: Appl. Phys.* **1979**, *12*, 1473−1484.

(44) Voinov, O. V. Hydrodynamics of wetting. *Fluid Dyn.* **1976**, *11* (5), 714−721.

(45) Cox, R. G. The dynamics of the spreading of liquids on a solid surface. Part1. Viscous flow. *J. Fluid Mech.* **1986**, *168*, 169−194.

(46) Lee, J. B.; Laan, N.; de Bruin, K. G.; Skantzaris, G.; Shahidzadeh, N.; Derome, D.; Carmeliet, J.; Bonn, D. Universal rescaling of drop impact on smooth and rough surfaces. *J. Fluid Mech.* **2016**, *786*, R4.